REPORT DOCUMENTATION PAGE

Form Approved
OMB No. 0704-0188

The public reporting burden for this collection of information is estimated to average 1 hour per response, including the time for reviewing instructions, searching existing data sources, gathering and maintaining the data needed, and completing and reviewing the collection of information. Send comments regarding this burden estimate or any other aspect of this collection of information, including suggestions for reducing the burden, to the Department of Defense, Executive Service Directorate (0704-0188). Respondents should be aware that notwithstanding any other provision of law, no person shall be subject to any penalty for failing to comply with a collection of information if it does not display a currently valid OMB control number.
PLEASE DO NOT RETURN YOUR FORM TO THE ABOVE ORGANIZATION.

1. REPORT DATE *(DD-MM-YYYY)*	2. REPORT TYPE		3. DATES COVERED *(From - To)*
19-12-2017	Final		26-09-2016 - 25-09-2017

4. TITLE AND SUBTITLE
Implanting Strong Spin-Orbit Coupling at Magnetoelectric Interfaces

5a. CONTRACT NUMBER

5b. GRANT NUMBER
HR0011-16-1-0005

5c. PROGRAM ELEMENT NUMBER

6. AUTHOR(S)
Jian Liu
Haixuan Xu

5d. PROJECT NUMBER

5e. TASK NUMBER

5f. WORK UNIT NUMBER

7. PERFORMING ORGANIZATION NAME(S) AND ADDRESS(ES)
University of Tennessee
Office of Sponsored Programs
1534 White Avenue
Knoxville, TN 37996-1529

8. PERFORMING ORGANIZATION REPORT NUMBER

9. SPONSORING/MONITORING AGENCY NAME(S) AND ADDRESS(ES)
Defense Advanced Research Projects Agency
675 North Randolph Street
Arlington, VA 22203-2114

10. SPONSOR/MONITOR'S ACRONYM(S)
DARPA

11. SPONSOR/MONITOR'S REPORT NUMBER(S)

12. DISTRIBUTION/AVAILABILITY STATEMENT
Approved for Public Release; Distribution Unlimited

13. SUPPLEMENTARY NOTES
The content of this report does not necessarily reflect the position or the policy of the Government.

14. ABSTRACT
The overarching goal of this work is to explore a new method for strong direct magnetoelectric (ME) coupling by creating acentric building blocks of spin-orbit-entangled states and incorporate them into ME nanostructures/devices. To test the feasibility of this approach, the focus of the supported one-year period is to address the question of how to design, synthesize and characterize the 2D ME structural unit. This question is the first step toward the ultimate goal of utilizing this 2D ME building block. The results of our first-principles calculations support the hypothesis of the proposed work that confining a 2D layer of strongly spin-orbit-coupled magnetic 5d elements in an interfacial environment would lead to ME effects larger than the conventional type-I multiferroics. A reliable computational procedure was established and applied to the prototype structure. The designed superstructures were synthesized and characterized. The key ingredients for the ME coupling were all implemented.

15. SUBJECT TERMS

16. SECURITY CLASSIFICATION OF:			17. LIMITATION OF ABSTRACT	18. NUMBER OF PAGES	19a. NAME OF RESPONSIBLE PERSON
a. REPORT	b. ABSTRACT	c. THIS PAGE			Jian Liu
U	U	U	UU		19b. TELEPHONE NUMBER *(Include area code)* 865-974-3055

Final Report: Implanting Strong Spin-Orbit Coupling at Magnetoelectric Interfaces

Jian Liu and Haixuan Xu
University of Tennessee

The overarching goal of this work is to explore a new method for strong direct magnetoelectric (ME) coupling [1] by creating acentric building blocks of spin-orbit-entangled states and incorporate them into ME nanostructures/devices. To test the feasibility of this approach, the focus of the supported one-year period is to address the question of how to design, synthesize and characterize the 2D ME structural unit. This question is the first step toward the ultimate goal of utilizing this 2D ME building block. For this purpose, the one-year supported period was broken down into two tasks. Each task consists of two components - DFT calculations and experiments.

Task One

The objectives of the DFT calculations are:
  i.   Perform survey on the stability of the polar structures with different cation combinations of the $AA'IrMO_6$ superlattices.
  ii.   Examine effect of epitaxial strain by fixing the lattice to possible substrates.
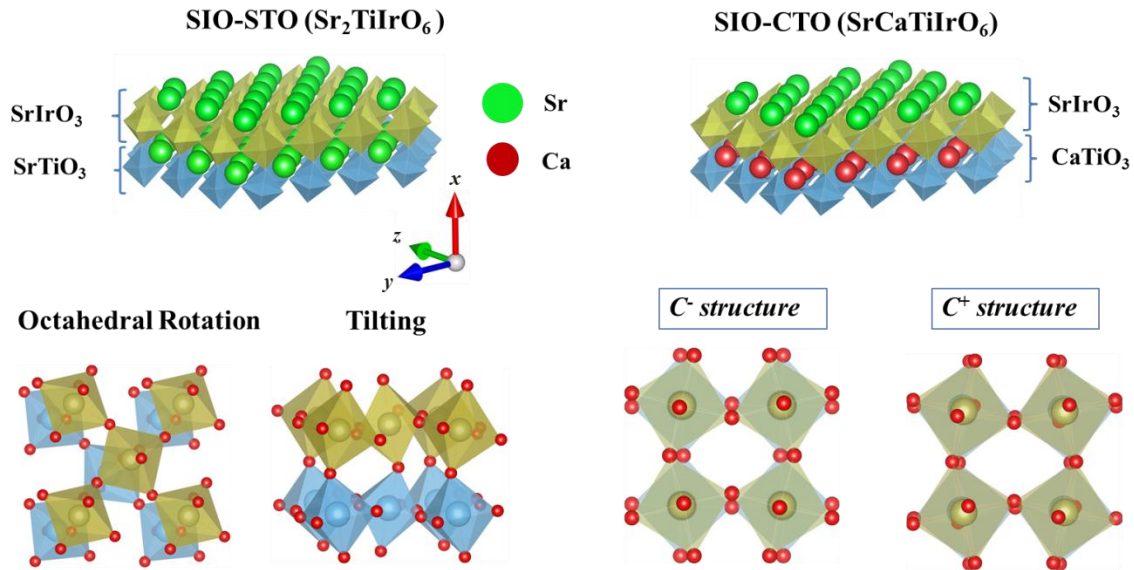 iii. Extract ME coupling from stable structures and identify promising combinations.

Figure 1. Top: the nonpolar (left) and polar (right) superlattice structures. Bottom: the octahedral rotation and tilting motions are highlighted on the left. The rotation in the two layers can be in-phase or out-of-phase as shown on the right. These two different structures are called c^+ and c^- structure, respectively.

Our calculations started with two cation combinations, A = A' = Sr and A = Sr & A' = Ca. In both cases, M = Ti. The first combination was designed to be nonpolar and serve as a

reference for the second one which was designed to be polar (Fig.1). In the rest of this report, we use x, y, and z for the unit cell, whereas a, b, and c are referring to the superlattice film structure. They can be mutually converted as x <-> c, y <-> a, and z <-> b. Stable structures were obtained for both combinations assuming growth on SrTiO3 substrate. As anticipated, the first combination was found to be nonpolar, while the second one is polar. Because the broken inversion symmetry in the polar structure is driven by a combination of the Sr-Ca cation mismatch and the octahedral rotation [2,3], we investigated different possible rotation patterns. It turns out the most stable rotation pattern is in-phase along the c-axis in the polar structure, whereas it is out-of-phase in the nonpolar structure. This difference is probably due to the cation size and cation motion, which is later confirmed by experiment.
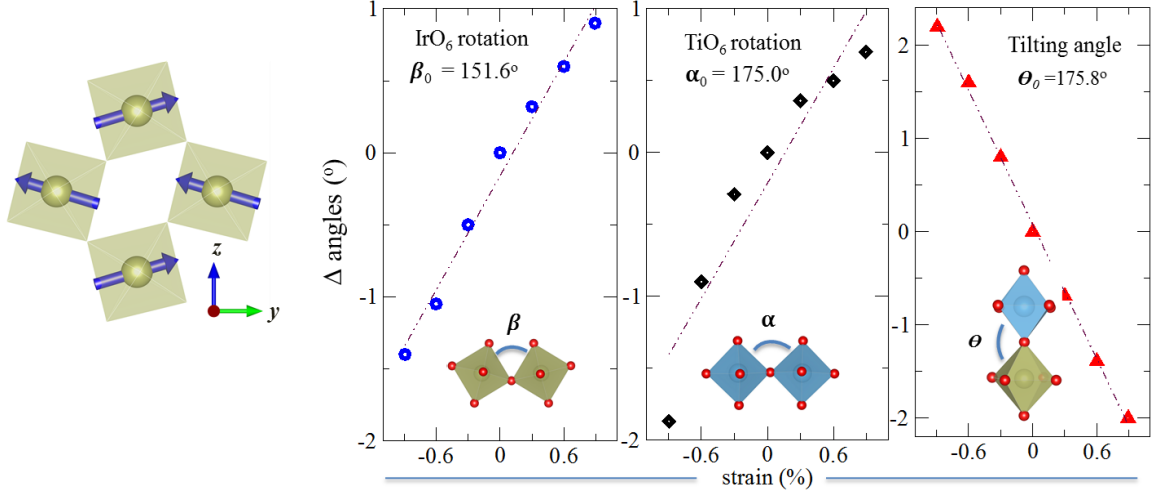

Figure 2. Left: a 2D unit cell with a canted antiferromagnetic structure. Right: changes of the rotation and tilting bond angles in the nonpolar structure as a function of strain.

In addition, both structures show a similar antiferromagnetic state with significant canting of the Ir moments (Fig. 2), which is consistent with the original design that the Ir ions provide the magnetic component for the ME coupling. The large canting is in line with the expectation that the strong spin-orbit coupling of the 5d element drives strong DM interactions. For the same reason, the canting is found to follow closely with the octahedral rotation patterns.
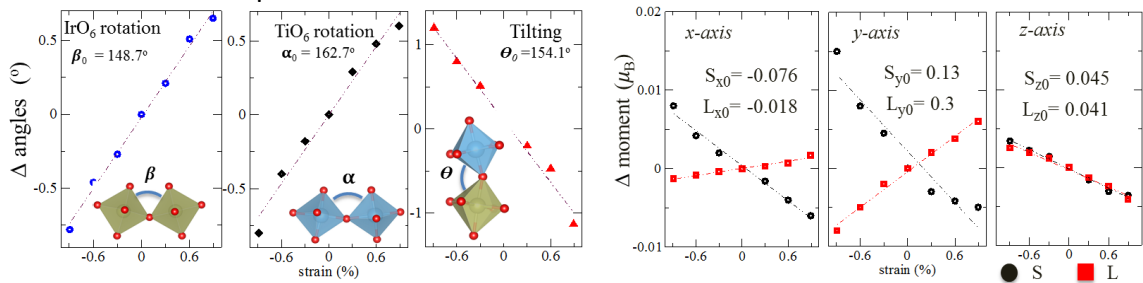

Figure 3. Left changes of the rotation and tilting bond angles in the polar structure as a function of strain. Right: the corresponding changes of the onsite moment.

Having established the stability and magnetic ground state of both the nonpolar and

2

polar structures, we investigated the strain effect to mimic the different lattice mismatches from various substrates. In both structures (Fig. 2 & 3), the planar Ir-O-Ir bond angle is found to increase from compressive to tensile strain, whereas the Ir-O-Ti bond angle decreases from compressive to tensile strain. Because of the strong spin-orbit coupling, the magnetic structure also follows these changes in the octahedral rotation pattern (Fig. 3).
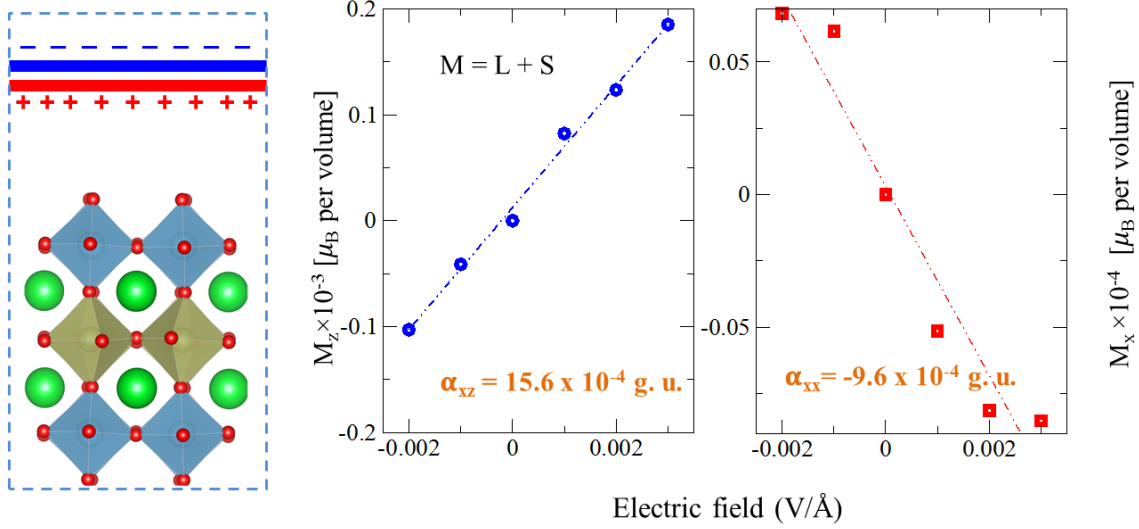

Figure 4. Left: a schematic of the slab configuration calculation. For clarity, only one layer of the slab is shown, whereas the entire slab consists of 13 layers. Middel & right: changes of magnetization of the polar structure along the z- and x-axis, respectively, as a function of the applied electric field along the x-axis.

Given the stable structures and their reasonable behavior under strain, we moved forward to calculate the ME coupling. A major challenge of this kind of calculation is that the spin and orbital degrees of freedom must be treated on an equal footing because of the strong spin-orbit coupling. We noticed that conventional methods based on first-principle calculations would only provide the spin component of the response. We thus developed two new methods to resolve this issue. The drawback is that including both spin and orbital is computationally more expensive than the conventional method and consume significantly longer time. Meanwhile, to ensure these new methods are reliable, we applied them to Cr2O3 as a benchmark system for comparison with literatures [4].

One of the methods is to construct a slab structure in VASP and apply an electric field across the slab to obtain the magnetic response. This method allows self-consistent treatment of spin-orbit coupling and hence includes orbital mediated ME coupling. The results of the ME coupling on Cr2O3 are consistent with values from literatures [4]. The results on the nonpolar structure show ME couplings with a similar magnitude to Cr2O3. This significant ME coefficient without breaking the inversion symmetry manifest a large boost of the ME effect with strong spin-orbit coupling. Results on the polar structure (Fig. 4) further shows a ME effect about one order larger than the nonpolar structure

3

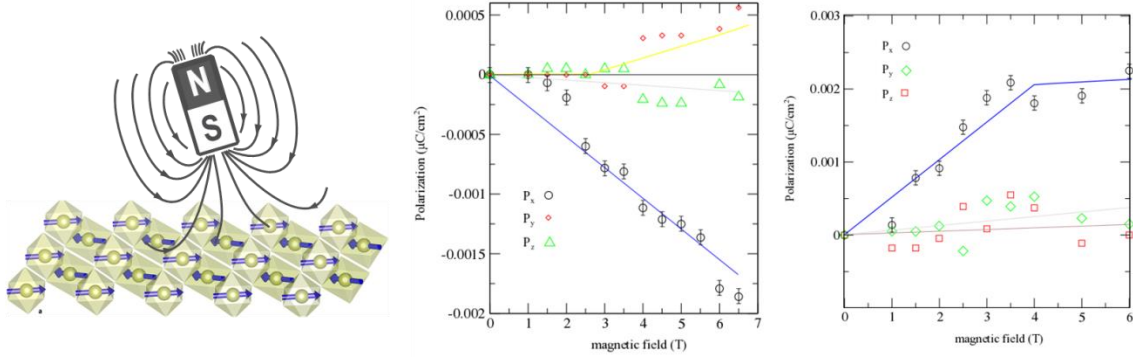and Cr2O3, in support of the original idea of the design.

Figure 5. Left: a schematic of the magnetic field-based calculation where the field can be applied to any direction. Middle and right: electric responses to a magnetic field applied along the x- and z-axis, respectively.

The second method is to apply magnetic field and calculate the electric response but in a different code - Abinit. This method extracts both ionic and electronic contributions that respond to the magnetic field via spin-orbit coupling. A deficit in the currently available code is that the magnetic field only couples to spins, while the orbital is considered via spin-orbit coupling. An advantage is however that the magnetic field can be applied to any direction, unlike the first method where changing the electric field direction requires constructing a new slab structure. This allows us to map out the entire ME matrix. At first, we obtained results qualitatively consistent with that under electric field from the first method. However, there were also significant quantitative differences. To refine our approach, calculations on Cr2O3 were performed to establish a benchmark. We found that obtaining a reliable ME matrix in this method requires a very high convergence standard for the zero field structure and a step-by-step increase of the field in the calculation. After getting a ME matrix of Cr2O3 consistent with both literature [4] and the electric field method, we applied the same procedure to the polar superlattice structure. The final ME matrix is in reasonable agreement with that from the electric field method and consistent with the polar point group symmetry of the structure. The ME matrices from the two methods are summarized in the unit of *ps/m* as following:

$$\text{ME- E-field} \begin{pmatrix} \alpha_{xx} & \alpha_{yx} & \alpha_{zx} \\ \alpha_{xy} & \alpha_{yy} & \alpha_{zy} \\ \alpha_{xz} & \alpha_{yz} & \alpha_{zz} \end{pmatrix} = \begin{pmatrix} -3.4 & * & * \\ 0 & * & * \\ 5.2 & * & * \end{pmatrix}$$

$$\text{ME B-field} \begin{pmatrix} \beta_{xx} & \beta_{yx} & \beta_{zx} \\ \beta_{xy} & \beta_{yy} & \beta_{zy} \\ \beta_{xz} & \beta_{yz} & \beta_{zz} \end{pmatrix} = \begin{pmatrix} -3.9 & 0.0 & 4.6 \\ 0.0 & 0.0 & 0.0 \\ -0.04 & 0.0 & 0.02 \end{pmatrix}$$

where α_{ij} and β_{ij} are the response coefficients to electric field and magnetic field, respectively. In principle, α_{ji} should be equal to β_{ij}. Indeed, we can see the correspondence between α_{xx} and β_{xx}, α_{xy} and β_{yx} as well as α_{xz} and β_{zx}. The magnetic field matrix has a number of very small coefficients near the calculation accuracy. After we approximate them as zero, the matrix has symmetry compatible with the symmetry

of polar magnetic structure.

In summary, the results of our calculations support the hypothesis of the proposed work that confining a 2D layer of strongly spin-orbit-coupled magnetic 5d elements in an interfacial environment would lead to ME effects larger than the conventional type-I multiferroics [3,4]. On the other hand, due to the importance of both the spin and orbital degrees of freedom, the calculations demand significant computational resources beyond our estimate to obtain reliable results. Therefore, we focused on establishing a reliable procedure and conclusion for the prototype structure and leave the test on other cation combinations for future study. Improving the computational efficiency in the future would also facilitate studies on this type of systems

The objectives of the experimental effort are:

  a. Prepare ablation targets and substrates for the growth of the AA'IrMO$_6$ superlattices with different combinations.
  b. Establish the layer-by-layer growth of AIrO$_6$ and A'MO$_3$ and find compatible growth conditions.
  c. Characterize and compare basic structural, chemical, and magnetic properties of the grown superlattices under both polar and nonpolar settings.
  d. Verify the stability of the polar structure and its impact to the spin-orbital moments.
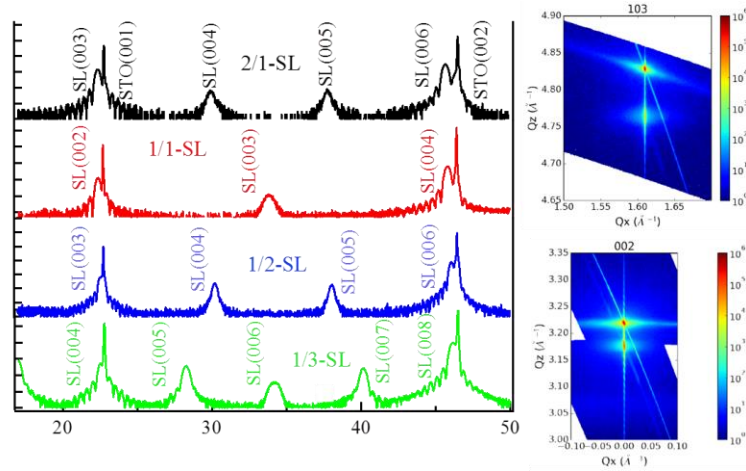 e. Probe ME responses under electric and magnetic fields

Figure 6. Left: Room temperature θ-2θ scans of the series of nonpolar superlattices (SLs). The corresponding superlattice peaks are also shown. Right: a representative reciprocal spacing mapping of the superlattice at the monolayer limit (1/1-SL) around the (103) and (002) (pseudocubic lattice) film peak.

To be in line with the DFT calculations, we focused on the two cation combinations, A = A' = Sr and A = Sr & A' = Ca with M = Ti in both cases (Fig. 1). In order to synthesize the superlatice structure by pulsed laser deposition, we prepared ablation targets of SrIrO3, SrTiO3 and CaTiO3. Substrate surface treatment was also performed prior to the growth.

We have successfully established the layer-by-layer growth of these materials under a compatible growth condition, which is necessary for building the superstructures.
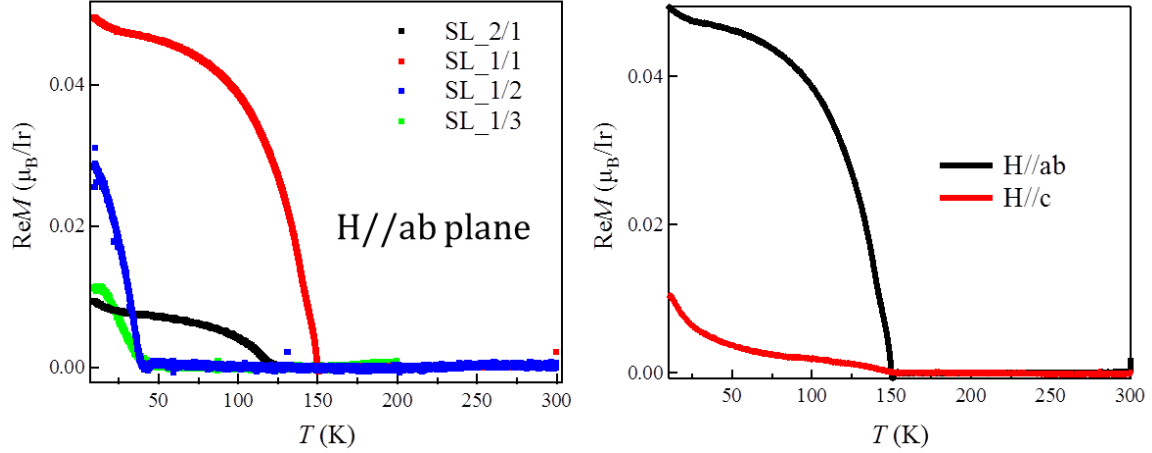

Figure 7. Left: The remnant magnetization plotted against temperature for the nonpolar superlattices in Fig. 6. Right: The remnant magnetization anisotropy between the in-plane and out-of-plane directions for the 1/1-SL, which is consistent with DFT calculation.

We first began with the nonpolar structure. Since the prototype structure design consists of monolayers of each of the two components, we experimentally approached to that limit by starting with growth of superlattices where the thickness of each layer is a few monolayers, and decreasing the layer thickness systematically. X-ray diffraction shows well defined superlattice peaks in correspondence with the growth control (Fig. 6). At the one monolayer limit of the superlattice, the Bragg peaks of octahedral rotation indicate an out-of-phase c-axis rotation pattern, consistent with the DFT result. X-ray absorption measurements showed the Ir4+ valence state as expected. Magnetometry identified magnetic phase transitions at various temperatures depending on the layer thickness in the superlattice (Fig. 7). The observed net magnetization is consistent with the DFT calculation which suggests a canted antiferromagnetic state. The large canting originates from the strong spin-orbit coupling of Ir.
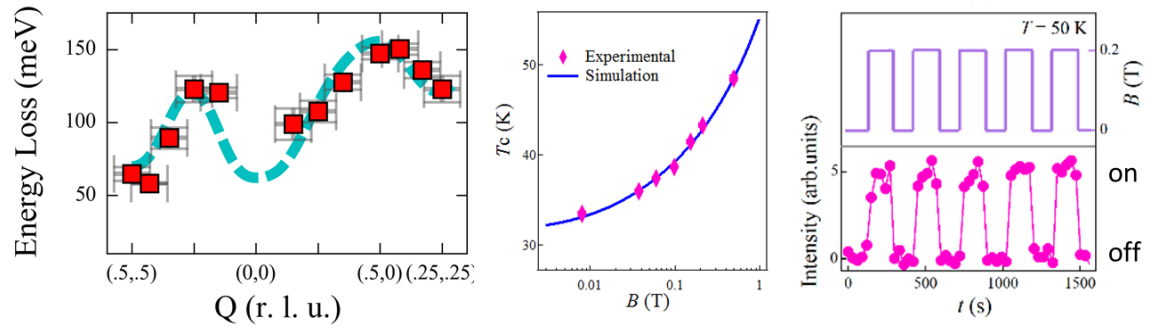

Figure 8. Left: The magnon excitation (red square) dispersion of the nonpolar 1/1-SL measured by RIXS. Dashed line is the fit to an antiferromagnetic spin Hamiltonian that yields the exchange coupling and DM interaction. Middle: The antiferromagnetic

6

transition temperature of the nonpolar 1/2-SL as a function of the magnetic field. Blue line is a fit to a logarithmic function. Right: The on/off switching of the antiferromagnetic diffraction peak of nonpolar 1/2-SL with a 0.2T field.

One interesting observation is that the transition temperature decreases as the SrTiO3 spacing layer increases from one to two, but remains more or less the same when it further increases to three (Fig. 7). This behavior indicates that, while isolating the 2D Ir layers weakens their mutual interaction and enhances 2D fluctuations, the intralayer interaction remains very strong to support finite temperature magnetic order. We performed resonant inelastic x-ray scattering (RIXS) to measure the magnon excitations (Fig. 8), which shows that the intralayer exchange coupling is ~50meV and the DM interaction is ~5meV. These are at least one order of magnitude large than that in ferrites for instance [3], confirming the critical role of spin-orbit coupling. The relatively low transition temperature compared with the strength of the exchange coupling is a result of the strong 2D fluctuations, which means that the layer has a large susceptibility. This is in line with our original idea that a 2D layer can host strong interactions and at the same time well respond to external coupling, such as interfacial effects.
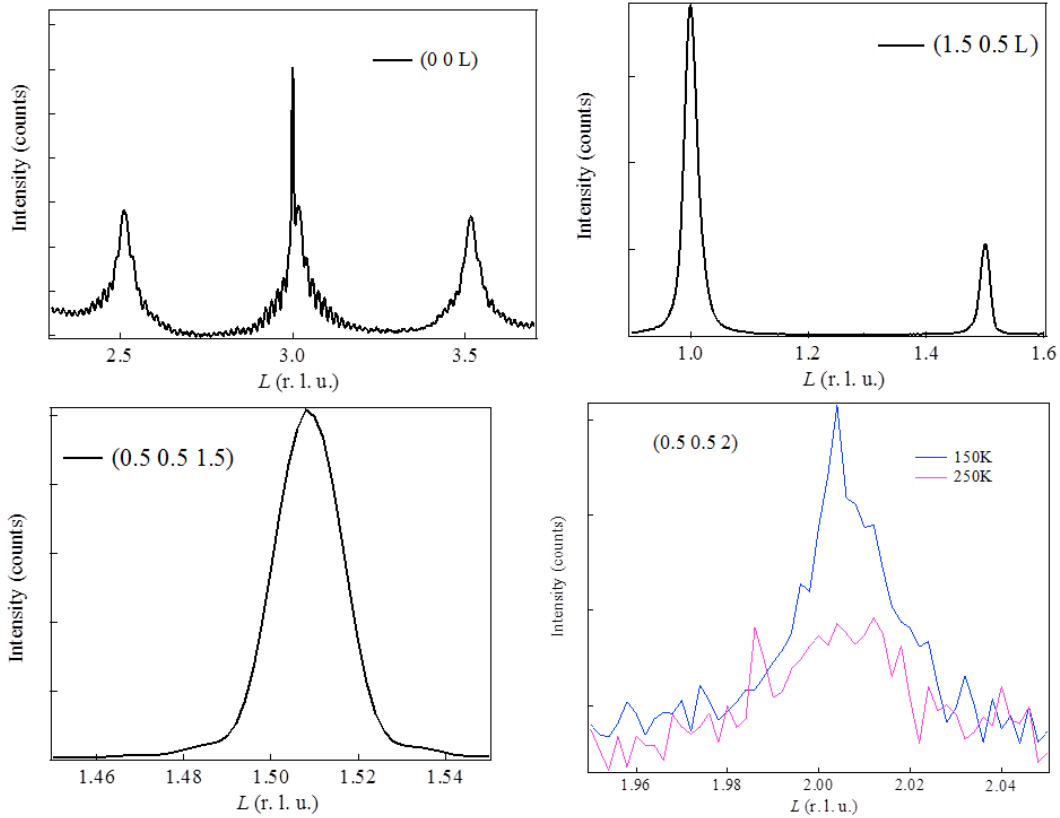

Figure 9. X-ray diffraction peaks for the polar superlattice structure (top left), its octahedral rotation (top right), octahedral tilt (bottom left), and cation off-centering motion (bottom right).

To confirm the canted antiferromagnetic state, we carried out resonant x-ray magnetic scattering, which directly probes the antiferromagnetic long-range order. The results are consistent with the expectations from magnetometry and DFT calculations. More interestingly, we found the antiferromagnetic order in superlattices with the thicker SrTiO3 spacer strongly responds to small external magnetic fields. Specifically, the ordering temperature logarithmically increases with the field by 50% at 0.5T (Fig. 8). This is remarkable considering that the Zeeman energy of such small field is three orders of magnitude smaller than the exchange coupling and two orders smaller than the scale of the ordering temperature. This extreme sensitivity allows us to turn on and off the antifferomagnetic order with a small field (Fig. 8). Further analysis suggests that this unexpected result is related to the combination of strong DM interactions and the strong 2D fluctuations. The former affords spin canting and a net moment for the antiferromgantic order to engage with the external field, whereas the latter leads to a large antiferromagnetic susceptibility. This result can open the door to new device mechanism based on antiferromagnets for faster and more secure processing.
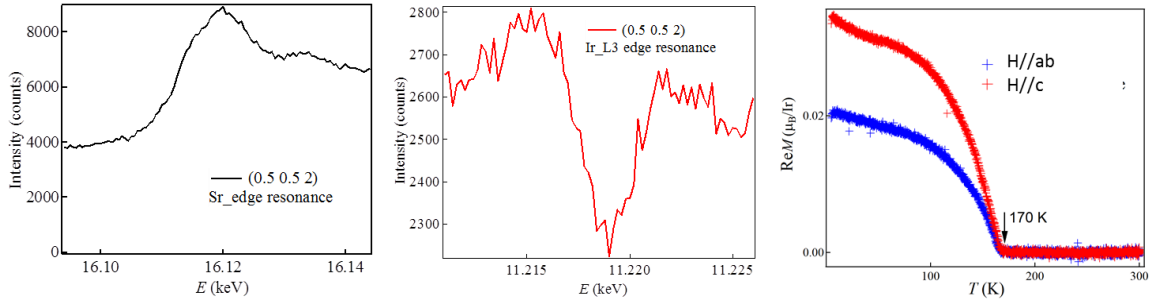

Figure 10. Resonant profile of the cation displacement peak across the Sr edge (left) and the Ir edge (middle). Right: The remnant magnetization plotted against temperature for the polar superlattices.

Having understood the nonpolar structure, we investigated the polar structure at the one-unit-cell thick limit. X-ray diffraction confirms the epitaxial superlattice structure (Fig. 9). The octahedral rotation shows a main peak at L = 1 and a weaker superlattice peak at L = 1.5 (Fig. 9), indicative of an in-phase c-axis octahedral rotation pattern, consistent with DFT calculations. We also found extra Bragg peaks of (0.5 0.5 L) with L = integer (Fig. 9), especially at lower temperatures, characteristic of the cation displacement from the original inversion center. These peaks are absent in the nonpolar structure and appear here due to the A-site ordering and the resulting inversion symmetry-breaking distortion. The peaks were found to have resonance both the A-site and the Ir site (Fig. 10), indicating the Ir site is asymmetrically displaced. These observations are in agreement with the structure stabilized in DFT calculations. The

8

magnetic ground state was also found to be a canted antiferromagnet. The out-of-plane canting of the spin-orbit moments is significantly enhanced (Fig. 10) compared with the nonpolar structure (Fig. 7), which can be a result of a larger octahedral tilting and the broken inversion symmetry as suggested in DFT calculations.
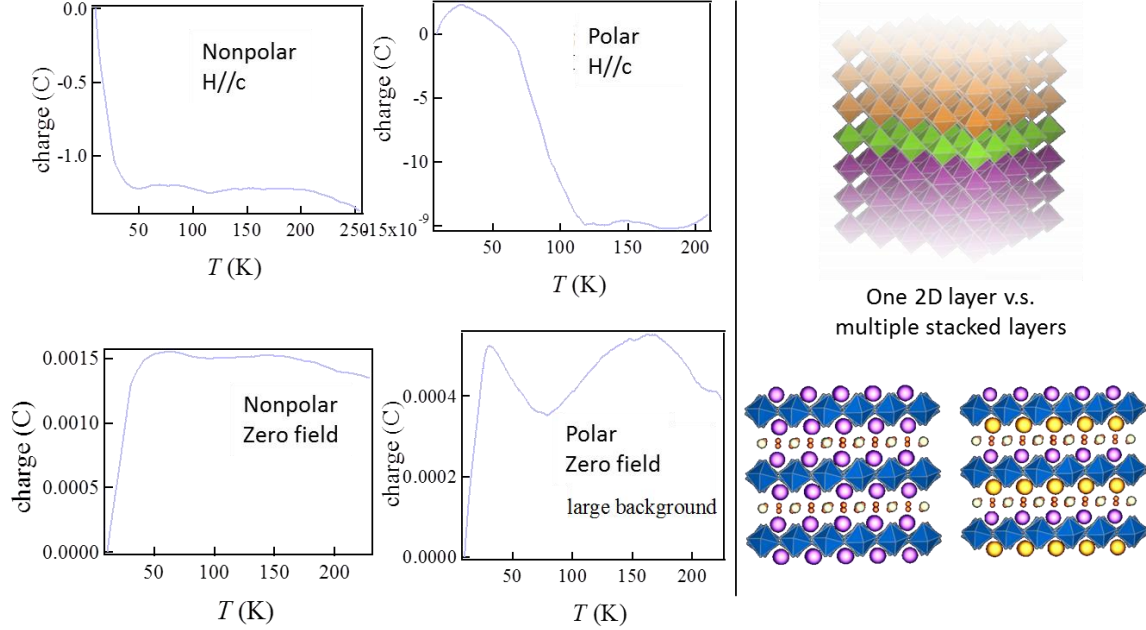

Figure 11. Left: Electric response as a function of temperature with and without the magnetic field for both the nonpolar and polar structures. Right: A schematic comparison between the superlattice structure of multiple 2D layers and the single 2D layer at an interface.

With the ground state properties established and in line with the original design, we attempted to performed preliminary characterizations of the ME effect. Because we encountered an unexpected prolonged down time of the instruments in our core facility, we seek alternative measurement setup and spent extra time to rewire and reprogram the cryostat of a local collaborator. Meanwhile, we also made devices on samples of the nonpolar structure. An array of closely spaced electrodes was made to enhance the signal. The drawback of this design is that the failing rate is relatively high because one shorted electrode will degrade the whole device. Nevertheless, we were able to test devices on both nonpolar and polar structures. While there appears to some large signal across the magnetic transition on the polar structure, the signal seems to be too large to be intrinsic (Fig. 10). The background signal on the device is also relatively large. We tested our measurement setup to exclude the possibility of an electronics issue. We suspect the large device signal is due to intrinsic loss of the structure. Although our original idea only requires one 2D layer to achieve the ME effect (Fig. 11), we designed the superlattice structure of multiple stacked layers so as to increase the sample volume

and enable all the characterizations. However, that may lead to leakage among layers and larger loss. While improving the sample quality is expected to help to some extent, a new design of a single-interface structure is likely necessary to exploit the ME effect.

In summary, we were able to synthesize and characterize the designed superstructures. The key ingredients for the ME coupling were all implemented. Results are consistent with DFT calculations. The direct measurement of the ME effect however encounters issues that are likely due to the multilayer structure. While indirect measurement will help identify the ME effect, an improved structure design would be needed in the future to address this problem.

Task Two

In addition to the Task 1, there is a secondary task (Task 2) during the one-year period, which was also broken down into two subtaskes, DFT calculations and experiments.

The objectives of DFT calculations:
   i.   Investigate the FE instability when replacing the $A'MO_3$ layer with $BaTiO_3$ and $PbTiO_3$ in the superlattices at different epitaxial strains.
   ii. Evaluate the associated impact on the ME effects.
   iii. Replace the M ion in the $A'MO_3$ layer with magnetic Cr, Mn, and Fe ions and examine the mutual impact between the magnetic orders of the 3d spin moments and the 5d spin-orbitals.

	Ba	Sr	Ti	Ir
Δc (Å)	0.04879	-0.04596	0.08671	-0.0115
Δa (Å)	0.00026	0.00119	0.00065	0.00026
Δb (Å)	0.00563	0.02108	0.05386	0.00022

We applied the calculation procedure developed in Task 1 to a superlattice structure where Ca is replaced with Ba. The obtained structural ground state indeed shows large polar displacement primarily from Ti (see table below) likely due to the FE instability of $BaTiO_3$. As a result, the Ir site is also significantly displaced from the inversion center. The magnetic ground state is a canted antiferromagnet, similar to the conclusion on the other structures from Task 1. However, because we had to spend extra time to develop the ME calculation method which is relatively computationally expensive as described in

the results of Task 1, we postponed the calculations for A' = Ba at different strains and the ME effect. For the same reason, we did not launch new calculation for the subtask iii in order to focus resources on solving the issues in the ME calculation methods and establishing the procedure.

Experiments:
   a. Prepare additional ablation targets and substrates (if needed).
   b. Synthesize heterostructures of the AA'IrMO$_6$ superlattices and a FE layer, such as BaTiO$_3$.
   c. Synthesize heterostructures of the AA'IrMO$_6$ superlattices and a FM layer, such as La$_{2/3}$Sr$_{1/3}$MnO$_3$.
   d. Characterize and compare basic structural, chemical, and magnetic properties of the grown structures with that developed in task 1.

We initiated the growth with A' = Ba. However, the initial results show the growth conditions developed for A' = Sr and Ca is not suitable for A' = Ba. The layering growth is not as stable and will need to be adjusted. Because of this issue and the extra time we had to spend on seeking the alternative ME measurement setup, we postponed the growth with La$_{2/3}$Sr$_{1/3}$MnO$_3$ to focusing Task 1.

Papers published in peer-reviewed journals:

Hao, L., Meyers, D., Frederick, C., Fabbris, G., Yang, J., Traynor, N., . . . Liu, J., Two-Dimensional J$_{eff}$=1/2 Antiferromagnetic Insulator Unraveled from Interlayer Exchange Coupling in Artificial Perovskite Iridate Superlattices. *PHYSICAL REVIEW LETTERS*, *119*(2), (2017). doi:10.1103/PhysRevLett.119.027204

Hao, L., Meyers, D., Dean, M.P.M., Liu, J. Novel spin-orbit coupling driven emergent states in iridate-based heterostructures, Journal of Physics and Chemistry of Solids, in press.

Manuscripts:

D. Meyers, Yue Cao, G. Fabbris, Neil J. Robinson, Lin Hao, C. Frederick, … Jian Liu, M. P. M. Dean, Magnetism in artificial Ruddlesden-Popper iridates leveraged by structural distortions. Nature Communications (submitted).

Lin Hao, D. Meyers, H. Suwa, J. Yang, C. Frederick, T. R. Dasa, … Jian Liu, Giant magnetic response of a two-dimensional antiferromagnet, Nature Materials (submitted).

T. Dasa, H. Lin, Jian Liu, H. Xu, Strain effects on structural and magnetic properties of SrIrO3/SrTiO3 Superlattice. In preparation.

Presentations:

Liu, J. (2017). Spin-Orbit Electronic and Magnetic States in 5d Oxide Heterostructures. American Physical Society March Meeting, New Orleans, Louisiana.

Hao, L., Meyers, D., Frederick, C., Yang, J., Dean, M., & Liu, J. (2017). Tuning intralayer and interlayer couplings in artificial layered structure of perovskite iridate. American Physical Society March Meeting, New Orleans, Louisiana.

Hao, L. (2017). Two-dimensional Jeff=1/2 Antiferromagnetism unraveled from interlayer coupling and controlled under external magnetic field. Condensed Matter Seminars, University of Tennessee, Knoxville, Tennessee.

References:

[1] Dzyaloshinskii, Sov. Phys. JETP 10, 628 (1960).
[2] N.A. Benedek, J.M. Rondinelli, H. Djani, P. Ghosez, and P. Lightfoot, Dalt. Trans. 44, 10543 (2015).
[3] S. Ghosh, H. Das, and C.J. Fennie, Phys. Rev. B 92, 184112 (2015).
[4] E. Bousquet et al. Phys. Rev. Lett. **106**, 107202 (2012).